ORIGINAL ARTICLE

Chemical structure characterization of polysaccharide from *Osmunda japonica* Thunb and its inhibitory activity on uterine fibroids

Xiaochen Liu, Xiaohong Yu *, Jingci Lyu, Fengwei Li, Yueling Shang, Yongmei Lyu, Jinbin Liu

School of Marine and Biology Engineering, Yancheng Institute of Technology, Yancheng, China

Abstract The active component polysaccharide of *Osmunda japonica* Thunb was extracted and its chemical structure was detected by FT-IR, 1D-NMR and 2D-NMR spectra, in order to have a positive preventive and therapeutic effect on uterine fibroids. The physicochemical properties of *Osmunda japonica* Thunb polysaccharides (OPP) were analyzed, and the results showed that OPP was heteropolysaccharides composed of six monosaccharides. Ara and Glc were the main monosaccharides of the polysaccharide, with a molecular weight of 252.54 ± 10.84 kDa. The main chain was connected by 1,3-linked Ara*f*, which had a high degree of branching, and was connected to the branch at the O-2 and O-3 positions. The mice model of uterine fibroids was established by the estrogen load method. The coefficient of the uterus in the mice model increased significantly, irregular nodular processes were observed in the uterus, focal hyperplasia appeared in the smooth muscle layer, cell enlargement, disordered arrangement of smooth muscle cells, and endometrial hyperplasia was obvious. Furthermore, this work found that the serum estradiol (E2) and progesterone (P) concentrations in the model group were significantly higher than those in the normal group ($P < 0.01$), indicating successful modeling. OPP decreased serum E2 and P levels in a dose-dependent manner. Collectively, OPP had an obvious inhibitory effect on uterine fibroids in estrogen-loaded mice.

* Corresponding author at: School of Marine and Biology Engineering, Yancheng Institute of Technology, Jianjun East Road 211, Tinghu District, Yancheng 224003, Jiangsu, China.
E-mail addresses: hotliuxiaochen@126.com (X. Liu), yxh1127@ycit.edu.cn (X. Yu).
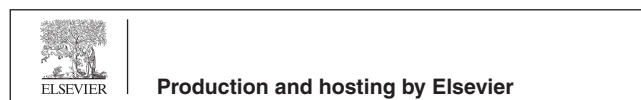
1. Introduction

Osmunda japonica Thunb is a young petiole of the perennial herb fern of the Osmundaceae (Tian et al., 2011). Its main components are polysaccharides and flavonoids. *Osmunda japonica* Thunb and its main components have anti-tumor and anti-cancer, anti-oxidation and anti-aging, anti-bacterial, anti-inflammatory, blood-activating, and stasis-resolving effects (Li and Shi, 2014). It is a kind of wild vegetable having medicine and food function with great development potential.

Many advanced scientific tools have been used to identify the molecular and structural characterization of polysaccharides. Fourier-transform infrared spectroscopy (FT-IR), 1D-NMR and 2D-NMR spectra are used to identify the functional ingredients of polysaccharides. Dai and Lei studied the monosaccharide composition and molar ratio of the OPP (Dai and Lei, 2001). The results showed that the OPP was composed of glucose (Glc), mannose (Man), xylose (Xyl), and galactose (Gal). The molar ratio of Glc, Man, Xyl, and Gal was 0.17:0.33:0.4:1. We also found that based on correlation analysis in previous studies, high uronic acid content, low molecular weight, and unique monosaccharide composition may be closely related to the strong antioxidant activity of OPP (Liu et al., 2020a,b,c). However, there are few reports on the finer structural characteristics of OPP.

At present, surgical resection is used as the radical method for the treatment of uterine fibroids, but drug control is still the first choice for patients who have fertility needs or do not meet the surgical conditions. Polysaccharides are mostly used for adjuvant treatment of tumors and have the advantages of good tumor suppression effect, high safety, and low toxic and side effects (Cui, 2012, Chen and Huang, 2017). Therefore, polysaccharides as an immune enhancer, adjuvant chemoradiotherapy has become an important means of tumor treatment. A large number of experimental studies have demonstrated that uterine fibroids are hormone-dependent tumors, and uterine fibroids are highly responsive to estrogen compared with normal myometrium (Boggess et al., 2020). Moreover, the levels of estrogen and progesterone in the serum secretory phase of patients with uterine fibroids are significantly higher than those in normal people (Nini et al., 2014). It is worth noting that the incidence of uterine fibroids in young women aged 20–30 is increasing year by year, due to the age of menarche and age of sexual maturity come early (Mohamed and Ayman, 2012). The research on the OPP is generally in the aspects of extraction, anti-oxidation, and bacteriostatic effects, and few studies have investigated its possible role in improving hormone-dependent diseases.

The mice model of uterine fibroids was established by the estrogen load method. After gastric perfusion of sample reagents, we observed the uterine pathological hyperplasia, uterine quality, serum estradiol (E2), and progesterone (P) levels in mice, and conduct histopathological studies. The purpose of this article is to provide a theoretical basis for the further development and utilization of *Osmunda japonica* Thunb, extract the active ingredient polysaccharide, and analyze its chemical structure, in order to have a positive preventive and therapeutic effect on uterine fibroids.

2. Materials and methods

2.1. Materials

Osmunda japonica Thunbs were obtained from Xinqing Forestry Bureau (Heilongjiang, China). D101 macroporous resin was acquired from Huayi Technology New Materials Co., Ltd. (Zhengzhou, China). Monosaccharide standards, including xylose (Xyl), rhamnose (Rha), arabinose (Ara), mannose (Man), glucose (Glc), and galacturonic acid (Gal A) standards, were purchased from Sigma-Aldrich (St. Louis, MO, USA). Dextrans of different molecular weights (T-10, T-40, T-70, T-110, T-500, and T-2000) were obtained from Zhenzhun Biotechnology Co. (Shanghai, China). Sodium Carboxymethyl Cellulose (CMC) was purchased from Ashland Chemical Co., Ltd. (Jiangmen, China). The serum estradiol (E2) kit (chemiluminescence immunoassay) and the serum progesterone (P) kit (chemiluminescence immunoassay) were obtained from Beckman Company (Indianapolis, Indiana, USA). Other chemicals and reagents were of analytical grade.

2.2. Extraction of OPP

The fresh and clean *Osmunda japonica* Thunb was dried to constant weight at 40 °C, ground, and then passed through 60 mesh sieve. After degreasing with methanol 3 times, it was filtered and the residue was dried to constant weight. The solid–liquid ratio was 1:50 and was extracted by 240 W microwave irradiation (microwave oven, Galanz Microwave Electric Co., Ltd.) for 1.5 min, and repeated 3 times. After filtration, the residue was discarded, and three volumes of 95 % ethanol were added to the solution, and the solution was allowed to stand for 24 h. The precipitate after centrifugation was vacuum freeze-dried to obtain a powdery sample. The sample (5 g) was dissolved in 250 mL of deionized water. The protein was removed by the Sevage method and decolorized with 25 % (30 % H_2O_2) in a water bath at 60 °C for 2 h. The treated solution was applied to a D101 macroporous resin column (2.0 cm × 30 cm) and eluted with a 40 % ethanol solution. The concentrated extract was poured into a dialysis bag (cut-off 8 kDa ∼ 14 kDa) and stirred with a magnetic stirrer for 24 h to replace the deionized water every 2 h. After dialysis, polysaccharides were further purified by three volumes of 95 % ethanol precipitation, centrifuge, vacuum freeze-drying, and named OPP.

2.3. Chemical analysis

The total sugar content in the polysaccharide sample was determined by the phenol-H_2SO_4 method using glucose as a standard (Tao and Tian, 2006). The uronic acid contents were determined by the m-hydroxydiphenyl method using galacturonic acid as a standard (Yuan et al., 2019). The molecular weight of the polysaccharide was determined by high-performance gel permeation chromatography (HPGPC) using a Waters Ultrahydrogel 2000 column (7.8 mm i.d. × 30 cm) equipped with a Shimadzu RID-10A refractive index detector. Dextrans (T-10, T-40, T-70, T-110, T-500, and T-2000) with different molecular weights were used as standards, and the pressure was maintained at 2.3 MPa.

The monosaccharide compositions of the polysaccharides were measured using high-efficiency liquid chromatography (HPLC). The PMP derivatives were analyzed on a Waters 2695 HPLC system equipped with a SinoChrom ODS-BP (C18) column (4.6 mm × 250 mm).

2.3.1. Methylation analysis

Methylation analysis of OPP was undertaken to ascertain the nature of the glycosidic bonding. According to a previously published method, 30 mg of the sample to be tested was methylated by treatment with a distilled NaOH/DMSO (Ji et al., 2018). After the sample was fully dissolved, CHI_3 (0.5 mL) was slowly added. Distilled water was added to terminate the reaction after 2 h. Complete methylation was confirmed by the disappearance of the O-H band (3200–3700 cm^{-1}) in the FT–IR spectrum (ALPHA-T, BRUKER Co., DE). The per-methylated OPP was treated with 3 mL 2 M trifluoroacetic

acid at 120 °C for 2 h. The excess formic acid was removed, and the methylated sample was converted to its corresponding alditol acetates by reduction with $NaBH_4$ at room temperature. The reduced polysaccharide was acetylated with acetic anhydride, then dissolved in chloroform for a GC–MS analysis on a GCMS-QP2010A instrument (Shimadzu Co., Ltd., Japan) equipped with an RTX-50 capillary column (30.0 m × 0.25 mm × 0.25 μm).

2.3.2. FT-IR and NMR spectrum analysis

The polysaccharide powders were pressed into KBr pellets. FT-IR spectra were recorded using an FT-IR spectrophotometer (ALPHA-T, BRUKER Co., DE) at 4000–500 cm^{-1} (Fimbres-Olivarria et al., 2018).

The polysaccharide was dissolved in deuterium water (D_2O, 99.9% D) and freeze-dried three times to replace any exchangeable protons with deuterium. The lyophilized sample was then dissolved in D_2O at a concentration of 20–30 mg/mL. All spectra were recorded using the pre-saturation suppression HOD method. ^1H NMR and ^{13}C NMR spectrum were used recorded Bruker AV III-500 NMR spectroscopy (Brucker, Rheinstetten, Germany) at 25 °C. COSY, HSQC, HMBC, and NOESY were detected by the state time proportional phase increment method.

2.4. Experimental animals

The experimental Kunming mouse (KM mice, strain code 202) was purchased from Beijing Weitong Lihua Experimental Animal Technology Co., Ltd., they were 5–8 weeks old, female, 18–22 g, SPF grade, and animal license number SCXK (Beijing, China) was 2016-0011. Mice were fed in cages under normal temperature and natural daylighting, and were free to drink and eat. The mice were subjected to adaptive feeding for > 5 days before gavage in each group of experiments. All experiments were performed in compliance with the author's institute's policy on animal use and ethics (Resolutions of the Northeast Agricultural University Ethics Committee on the Use of Live Animals in Teaching & Research, No. 20180421).

2.5. Preparation of samples and reagents

OPP: light yellow powder. 200 g was weighed, ground and 5 % CMC was added to prepare a 20 mL suspension at a concentration of 10 mg/mL. Take appropriate amount of suspension and dilute to 5 mg/mL and 2.5 mg/mL respectively.

Diethylstilbestrol: 0.5 mg/tablet, produced by Shanghai Xinyi Kangjie Pharmaceutical Co., Ltd., license No. H31020555. Four tablets (2 mg) were ground and 5 % CMC was added to make a 4 mL suspension at a concentration of 0.5 mg/mL. Each 10 mL sample was mixed with 0.1 mL diethylstilbestrol suspension and then administered.

Levonorgestrel: 0.75 mg/tablet, produced by Huarun Zizhu Pharmaceutical Co., Ltd., license No. H10983129. A 50 mL suspension was prepared by grinding 1 tablet (0.75 mg) and adding 0.5 % CMC. The concentration was 0.015 mg/mL.

Guizhifuling: Capsule, produced by Jiangsu Kangyuan Pharmaceutical Co., Ltd., license No. Z10950005. Take 1 capsule and pour out the contents (0.3 g) for grinding. Add 0.5 % CMC to make 12 mL suspension at a concentration of 25 mg/mL.

2.6. Model preparation and grouping modeling method

Among the many modeling methods, this study used Ma Jun et al. and Zeng Tao et al. to model exogenous estrogen-loaded animals (Ma Jun et al., 2008, Tao, 2011).

Female mice weighing about 20 g were randomly divided into 7 groups of 8 animals each. Except for the normal group, the other groups were given diethylstilbestrol-containing drugs by gavage. The model was created and administered intragastrically. The solvents were all 0.5 % CMC. (1) Normal group: 0.5 % CMC (no diethylstilbestrol added); (2) Model group: 0.5 % CMC; (3) Levonorgestrel group: 0.3 mg/kg; (4) Guizhifuling group: 500 mg/kg (5) OPP low-dose group: 50 mg/kg (6) OPP medium-dose group: 100 mg/kg; (7) OPP high-dose group: 200 mg/kg.

20 mL/kg was given by gavage regularly every day for 9 consecutive days. The animals were weighed every two days to observe their weight changes and to adjust the dosage according to their weight. The mice were sacrificed by cervical dislocation at 24 h after the last administration, and the uterus was weighed.

$$Uterine\ coefficiednt = \frac{Uterine\ weight}{mice\ weight} \times 1000$$

2.7. Uterine morphology examination

The bilateral uterus was fixed in the formaldehyde solution, and the sections at the maximum diameter of the roots of the bilateral uterus were taken separately, and the conventional methanol was dehydrated, embedded in paraffin, and stained with Hematoxylin-eosin staining (H). Morphological changes of the uterine muscle wall and endometrial gland in each animal of each group were observed under the light microscope (Olympus optical microscope, Tokyo, Japan).

2.8. Detection of serum E2 and P

Another batch of female mice, 8 in each group, was modeled and administered in the same manner for 15 consecutive days. 40 min after the last administration, the mice were subjected to pick off the eyeballs with ophthalmology forceps, and after the blood was taken, the mice were sacrificed by cervical dislocation. After the blood was allowed to stand at room temperature for 20 min, the serum was taken at 2000 r/min, centrifuged for 10 min, and the concentrations of estradiol (E2) and progesterone (P) were determined by chemiluminescence immunoassay according to the kit requirements.

2.9. Statistical analysis

The data were statistically analyzed using Prism 7.0 statistical software. The analysis results were all represented by $\bar{X} \pm S$. The data conformed to the normal distribution and the homogeneity test of variance was analyzed by one-way analysis of variance (Oneway-ANOVA). Non-parametric tests are used for data that does not conform to a normal distribution. $P < 0.01$ was very significant, and $P < 0.05$ was considered statistically significant.

3. Results and discussion

3.1. Chemical analysis

The total sugar content and uronic acid content (79.91 ± 0.28 % and 9.17 ± 0.41 %, respectively) of the polysaccharide are shown in Table 1. In the study of Dioscorea polysaccharides, it was found that the polysaccharides extracted by hot water extraction method had higher molecular weight (1004.2 kDa), while the polysaccharides extracted by ultrasound-assisted extraction method had smaller molecular weight (40.3 kDa) and the strongest antioxidant activity (Zhao et al., 2017). Microwave-assisted extraction technology was employed for OPP. Its molecular weight is 252.54 kDa, which is relatively large, but has strong antioxidant activity, antibacterial activity and functional properties (Liu et al., 2020a,b,c, Liu et al., 2021). In addition, no protein was detected, re-examination was performed with an ultraviolet spectrometer (Shimadzu UV-2450, Japan), and no absorbance was found at 260 nm and 280 nm. The natural polysaccharides isolated from *Osmunda japonica* Thunb have been reported to contain four monosaccharides, Glc, Man, Xyl, and Gal (Dai and Lei, 2001). This work identified six monosaccharides, most likely due to differences in the extraction methods. Notably, Ara and Glc are the main monosaccharides of the polysaccharide obtained herein. Therefore, OPP was a heteropolysaccharide composed of six monosaccharides with a molecular weight of 252.54 ± 10.84 kDa.

3.1.1. Methylation analysis of OPP

Based on the results of the GC–MS and mass spectrometry fragment analysis were shown in Table 2, the main configuration of the sugar residues in the OPP was deduced. OPP was mainly composed of T-Ara$f$ (11.16%), 1,3-linked Ara$f$ (4.47%), 1,3,5-linked Ara$f$ (26.54%), 1,2,5-linked Ara$f$ (12.62%),T-Glc$p$ (9.21%), and 1,6-linked Glc$p$ (17.32%). The residues of Ara mainly exist in the form of T-Ara$f$, 1,3-linked Ara$f$, 1,3,5-linked Ara$f$ and 1,2,5-linked Ara$f$, among which the contents of 1,3,5-linked Ara$f$ and 1,2,5-linked Ara$f$ were high, indicating that the branching degree of OPP was high. Moreover, the residues of Glc mainly exist in the form of T-Glc$p$ and 1,6-linked Glc$p$, and a small amount of them exist in the form of 1,4-linked Glc$p$, and 1,3,6-linked Glc$p$. Other residue types mainly include 1,4-linked Xyl$p$, 1,3,4-linked Xyl$p$, 1,3,4-linked Gal$p$, T-Rha$p$, 1,3-linked Rha$p$, and 1,4-linked Gal$p$, etc. (He et al., 2020, Ji et al., 2020, Yang et al., 2020). Therefore, the main chain of OPP was connected in a 1,3-linked Ara$f$ manner, and its branching degree was relatively high. According to the previous literature, the greater the branching degree, the stronger the biological activity (Zhao et al., 2019). These results suggest that the OPP may be considered as a branched polysaccharide, and it was connected to the branch chain at the O-2 and O-3 positions. On the other hand, since T-Ara$f$ and T-Glc$p$ were relatively large in proportion, they were mainly at the end of the main chain. The ratio obtained here agreed overall with the monosaccharide composition of OPP from the GC analysis.

Table 1 Chemical components of OPP.

Samples	Total sugars content (%)	Protein (%)	Uronic acid (%)	Mw (kDa)	Monosaccharide composition (mol%)					
					Ara	Rha	Gal A	Glc	Xyl	Man
OPP	79.91 ± 0.28	ND	9.17 ± 0.41	252.54 ± 10.84	53.28 ± 1.00	4.13 ± 0.10	3.17 ± 0.14	32.51 ± 0.59	1.25 ± 0.11	5.67 ± 0.08

Data are expressed as the mean ± SD.
Mol % is given based on the total content of the monosaccharide (Ara, Rha, Man, Glc, Xyl, and GalA).
ND: Not detected.

Table 2 Methylation analysis results of polysaccharide.

Glycosidic bond type	Main fragment (m/z)	Relative ratio (%)
T-Ara$f$	43, 59, 71, 87, 101, 117, 129, 145, 161	11.16
1,3-linked Ara$f$	43, 87, 99, 113, 118, 129, 189, 233	4.47
1,3,5-linked Ara$f$	43, 85, 99, 117, 127, 159, 261	26.54
1,2,5-linked Ara$f$	43, 59, 71, 87, 88, 129, 130, 189, 190	12.62
T-Glc$p$	43, 71, 87, 101, 117, 129, 145, 161, 205	9.21
1,4-linked Glc$p$	43, 71, 87, 99, 101, 117, 129, 131, 161, 173, 233	1.61
1,6-linked Glc$p$	43, 87, 101, 117, 129, 145, 161, 173, 189, 217, 233	17.32
1,3,6-linked Glc$p$	43, 87, 99, 117, 129, 141, 173, 189, 201, 245, 305	2.87
1,4-linked Xyl$p$	43, 71, 87, 101, 117, 129, 161, 189, 233	1.59
1,3,4-linked Xyl$p$	43, 99, 117, 129, 159, 189, 201, 261	1.03
1,3,4-linked Gal$p$	43, 99, 117, 129, 189, 201, 245, 261, 305	1.81
T-Rha$p$	43, 61, 71, 87, 101, 117, 129, 161, 219	1.78
1,3-linked Rha$p$	43, 71, 87, 89, 129, 131, 175, 189	3.79
1,4-linked Gal$p$	43, 71, 87, 99, 101, 117, 129, 131, 161, 173, 233	1.68

From the above results, it can be seen that the structure of OPP was relatively complicated, and the main chain part was continued to be methylated to obtain a finer internal structure of OPP. The methylation analysis was hydrolyzed with 0.1 M TFA, and the components in the dialysis bag were collected as the main chain part OPP-1 of the polysaccharide. The results of further methylation analysis of OPP-1 were shown in Table 3. 1,3-linked Ara*f* (27.84%) was the main residue of OPP-1, indicating that this residue should be on the main chain of OPP-1. Since the relative ratio of 1,3,5-linked Ara*f* decreased from 26.54% to 12.44%, it may be that the 1,3-linked Ara*f* of OPP-1 was mainly converted from 1,3,5-linked Ara*f*. In addition, T-Ara*f* (20.32%) and T-Glc*p* (4.21%) were the main terminal residues of OPP-1, and the content of Glc*p* decreased significantly, which may be due to the connection of some 1,6-linked Glc*p* residues of OPP-1 with the main chain through 1,3,5-linked Ara*f*.

3.1.2. FT-IR spectroscopic analysis

The FT-IR spectrum has polysaccharide-specific bands in the range of 4000–400 cm^{-1} (You et al., 2014). As shown in Fig. 1A, the broadband at 3346.27 cm^{-1} represented the characteristic peak of hydrogen-bonded O—H stretching vibrations, the bands at 2933.73 cm^{-1} were indicative of C—H antisymmetric stretching vibrations. The bands observed at 1608 and 1439 cm^{-1} in the OPP fraction were attributed to the absorption of deprotonated carboxylic groups, which indicated the presence of uronic acids (Wang, 2014). Furthermore, according to the position of the infrared absorption peak, the configuration of the glycosidic bond can be determined (Wierman, 2019). The absorption band at 921 cm^{-1} was indicative of β-pyranose, and that at 829 cm^{-1} was indicative of α-pyranose.

3.1.3. NMR spectroscopic analysis

One dimensional NMR (^{1}H NMR and ^{13}C NMR) was used to analyze the glycosidic bonds and anomeric protons in OPP. In the ^{1}H NMR spectra δ 3–5.5 PPM signal is the characteristic peak of polysaccharide, usually the chemical shift of α configuration is δ5.0–5.5 ppm, β configuration is δ4.0–5.0 ppm (Wan and Fang, 2000). The signal of saccharide ring was in the range of δ3.5–3.8 ppm, the signal of β-Glc was in the range of δ4-5 ppm, and the signal of 5.5–5.0 ppm was assigned to α-Ara*f* residues (Fig. 1B), which was consistent with the main

glycosidic bonds shown by IR and GC analysis. Further, the peak appearing at δ 3.64 ppm corresponds to the —O—CH$_3$ part. δ1.0–1.15 ppm was the signal of the methyl proton at the Rha*p*6 position, and near δ2.0 ppm was the characteristic peak of the acetyl group on galacturonic acid. In the ^{13}C NMR spectrum, the signal in the range of δ60-80 ppm was the characteristic peak of C2-C6, and the signal at δ174.5 ppm can be attributed to uronic acid (Chen et al., 2020).

To obtain the fine structure information of OPP, the main chain part OPP-1 obtained by its hydrolysis was analyzed by methylation reaction derivatives, and the structure of different polysaccharide residues and their ratios were determined. Based on the integration of the main abnormal proton signals, we also identified different polysaccharide residues. In these two groups of ratios (Tables 4 and 5), we found data with similar proportions to determine the corresponding polysaccharide residues in different hydrogen atoms in the NMR spectrum, and then determined different polysaccharide residues by HSQC (Fig. 2C) and COSY (Fig. 2A) spectrum. Finally, the glycosidic bonds between saccharide groups were determined by two-dimensional correlation spectra such as HMBC (Fig. 2D), COSY, and NOESY (Fig. 4B). According to the ^{1}H NMR spectrum (Fig. 1C), OPP-1 had four main abnormal proton signals at δ5.03, 5.16, 5.23, and 4.91, which were marked A, B, C, and D, respectively. Based on the abnormal positions of carbon and hydrogen signals, these four saccharide groups were arabinose in α configuration. The ^{1}H NMR and ^{13}C NMR of all marked residues were assigned with the data of COSY, HSQC, and NOESY spectra. Some residue connections were observed in the HMBC spectrum: A H1-C C4, B H1-C C4, B H1-C C3, C H1-A C4, C H1-D C4, and D H1-A C4. Based on the above analysis, it is inferred that the structure of the OPP is shown in Fig. 3.

At present, scholars have found that most of the wheat bran polysaccharides are arabinoxylan, which mainly consisted of xylan backbone linked by (1 → 4)-β-D-Xyl*p* units with the O-2 or O-3 positions substituted with arabinose, glucose and galactose residues, and the glycoside bonds that comprise the side chains of polysaccharides include T-α-Ara*f*, 1,2-α-Ara*f*, 1,3-α-Ara*f*, T-Gal*p*, and α-D-GlcA (Marquez-Escalante et al., 2018, Liu et al., 2020a,b,c). And it is believed that the hot water extracted polysaccharides mostly consisted of Glc, while the major monosaccharide residue of alkali-extracted polysaccharides was Ara and Xyl (Lv et al., 2021). The results

Table 3 Methylation analysis results of OPP-1.

Glycosidic bond type	Main fragment (m/z)	Relative ratio (%)
T-Ara*f*	43, 59, 71, 87, 101, 117, 129, 145, 161	20.32
1,3-linked Ara*f*	43, 87, 99, 113, 118, 129, 189, 233	27.84
1,3,5-linked Ara*f*	43, 85, 99, 117, 127, 159, 261	12.44
1,2,5-linked Ara*f*	43, 59, 71, 87, 88, 129, 130, 189, 190	11.32
T-Glc*p*	43, 71, 87, 101, 117, 129, 145, 161, 205	4.21
1,6-linked Glc*p*	43, 87, 101, 117, 129, 145, 161, 173, 189, 217, 233	7.32
1,4-linked Xyl*p*	43, 71, 87, 101, 117, 129, 161, 189, 233	1.38
1,3,4-linked Xyl*p*	43, 99, 117, 129, 159, 189, 201, 261	0.83
T-Rha*p*	43, 61, 71, 87, 101, 117, 129, 161, 219	2.68
1,3-linked Rha*p*	43, 71, 87, 89, 129, 131, 175, 189	1.65
1,4-linked Gal*p*	43, 71, 87, 99, 101, 117, 129, 131, 161, 173, 233	1.67

Fig. 1   FT-IR spectrum in the 4000–400 cm^{-1} region of OPP (A). NMR spectra (^{1}H NMR and ^{13}C NMR) of OPP (B). NMR spectra (^{1}H NMR and ^{13}C NMR) of OPP-1 (C).

were different from the monosaccharide compositions of OPP in the present study, and the major monosaccharide residue were also different, which may be due to different extraction materials and separation methods. Comparing with the literature, the OPP in this manuscript, is a novel polysaccharide that never reported.

3.2. Effects on mice body weight and uterine weight

As can be seen from the results (Table 6), the average body weight of each group of mice was increased compared with that before administration (first day). Compared with the normal group, the uterus coefficient of the model group increased

Table 4　Residue chemical shift assignments in OPP-1.

Residues		1	2	3	4	5	6
A	C	109.19	79.07	70.02	68.07	60.85	
1,3-linked Ara*f*	H	5.03	4.25	4.11	3.84	3.62	
B	C	100.15	79.20	73.52	71.14	67.67	
T-linked Ara*f*	H	5.16	4.27	3.78	3.63	3.53	
C	C	100.45	79.34	73.39	71.14	67.67	–
1,3,5-linked Ara*f*	H	5.23	4.25	3.77	3.62	3.51	3.41
D	C	101.12	79.12	68.31	60.63	67.85	
1,2,5-linked Ara*f*	H	4.91	4.23	3.81	3.61	3.51	

Table 5　Connection information of anomeric hydrogens and anomeric carbons on OPP-1 residues in HMBC.

Residues		H1/C1	Observed connectivities		
		$\delta H/\delta C$	$\delta H/\delta C$	Residue	Atom
A	1,3-α-linked Ara*f*	5.03	71.14	C	C4
		109.19	3.61	D	H4
B	T-α-linked Ara*f*	5.16	71.14	C	C4
		79.34	4.25	C	H2
		100.15	68.31	D	C3
C	1,3,5-α-linked Ara*f*	5.23	68.07	A	C4
			60.63	D	C4
		100.45	3.61	D	H4
D	1,2,5-α-linked Ara*f*	4.91	68.07	A	C4
		101.12	3.61	D	H4

significantly ($P < 0.01$), indicating successful modeling (Fig. 5A). After modeling and drug intervention, compared with the model group, the uterus coefficient of the high, medium, and low dose groups of OPPs decreased, with a significant difference ($P < 0.01$). The uterine coefficient of the high-dose group and levonorgestrel was not significantly different from that of the normal group. The positive control drugs levonorgestrel and Guizhifuling reduced the uterus coefficient, and the difference was also significant compared with the model ($P < 0.01$).

It has been reported that the efficacy of the Guizhifuling capsule is similar to that of the Guizhifuling pill, which has maintained the efficacy of traditional pills (Qi et al., 2016). Li Dongyun applied Guizhifuling capsule to treat 60 cases of uterine fibroids. After 3 months, 55 cases were effective, and the effective rate was 91.67 % (Dongyun, 2010). In this study, the Guizhifuling capsule was selected as the positive control drug for traditional Chinese medicine. The results showed that the anti-proliferative effect of the high-dose group was better than that of the Guizhifuling group. It indicated that it had the potential to be a substitute for anti-hysteromyoma drugs.

Although there is no evidence that estrogen directly stimulates the growth of fibroids, the high sensitivity of fibroids to estrogen plays an important role in its pathogenesis (Liao et al., 2019). Therefore, estrogen modeling is a more common method. The basic principle is that estrogen has a mitogenic effect, which can stimulate progesterone receptors, epidermal growth factors, and insulin-like growth factors to cause fibroid growth (Fan et al., 2019). It was initially shown that OPP significantly inhibited the uterine fibroids-like proliferation induced by diethylstilbestrol in a dose-dependent manner.
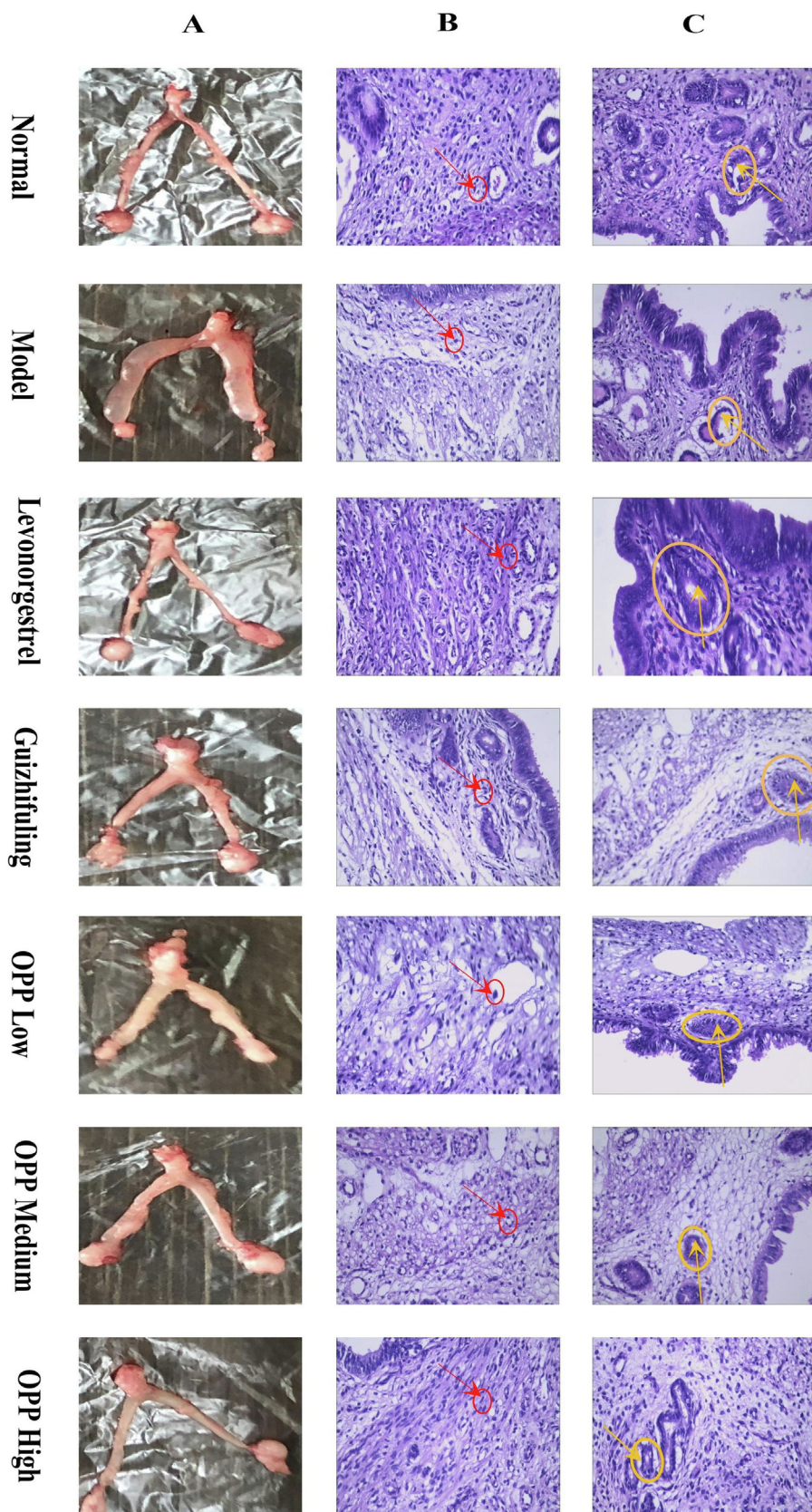
3.3. Morphological changes in the uterus

The uterus of the normal group was slender and the texture was smooth. In the model group, the uterus of the mouse was hypertrophied, and most of the irregular nodules were visible. The uterine morphology of levonorgestrel, Guizhifuling, and OPP high-dose groups was similar to that of the normal group, while irregular nodules appeared in the uterus of the OPP low-dose group and medium dose group (Fig. 4A). Dai Jinfeng and Li Lei, etc. extracted the water-soluble OPP (Dai Jinfeng et al., 1999, Li Lei, 1999). At the same time, they also proved that OPP had multiple functions such as pain relief, muscle regeneration, and skincare, while it was anti-bacterial and anti-inflammatory effects. This was because the colloidal solution in which the OPP had dissolved forms a protective layer on the surface of the cell or body, thereby restoring the function of the inflamed mucosa or cells and the disturbed mucus layer. The anti-inflammatory, detumescence, and analgesic effects of OPP may also alleviate the early symptoms of uterine fibroids, thus making the uterine morphology of the OPP high-dose group closer to the normal group.

3.4. Arrangement of smooth muscle cells

Due to uterine fibroids are mainly formed by the proliferation of uterine smooth muscle cells, disordered smooth muscle cell arrangement and abnormal endometrial morphology are early symptoms of uterine fibroids. Fig. 4B showed the regular arrangement of uterine muscle fibers in the normal group of mice. The uterine smooth muscle layer was thin and has no

Fig. 2 COSY spectra (A), NOESY spectra (B), NOESY spectra (C), and HMBC spectra (D) of OPP-1.

Fig. 3 The structural composition of OPP. R may be 1,4-linked Xyl*p*, 1,3,4-linked Xyl*p* and 1,3,4-linked Gal*p*.

Fig. 4 Uterine morphology of mice in each group after 9 days of diethylstilbestrol induction and drug intervention (A), arrangement of mouse uterine smooth muscle cells in each group (B), endometrial glands in each group of mice (C).

Table 6 Comparison of body weight and uterine weight in mice.

Group	First day	Third day	Fifth day	Seventh day	Ninth day	Uterine weight (g)
Normal	18.19 ± 0.91**	22.25 ± 0.83**	24.40 ± 0.89*	24.93 ± 0.58	25.12 ± 0.76	0.25 ± 0.02**
Model	22.17 ± 0.58##	25.05 ± 0.66##	24.83 ± 1.71	24.51 ± 1.44	25.15 ± 1.42	0.52 ± 0.10##
Levonorgestrel	21.67 ± 0.66##	24.65 ± 0.91##	26.78 ± 0.78	26.28 ± 0.98	28.19 ± 1.37	0.28 ± 0.02**
Guizhifuling	20.98 ± 0.93##	23.81 ± 0.68	26.49 ± 0.77	26.74 ± 1.84	27.19 ± 1.23	0.38 ± 0.05*
OPP low dose	21.73 ± 1.43##	23.54 ± 0.91	28.04 ± 1.88#*	27.96 ± 2.02*	29.60 ± 2.42#*	0.45 ± 0.15##
OPP medium dose	17.97 ± 1.01**	22.27 ± 1.01**	25.74 ± 2.00	25.37 ± 1.86	25.95 ± 2.23	0.34 ± 0.03*
OPP high dose	22.21 ± 0.73##	25.35 ± 0.83##	27.71 ± 1.94#	28.16 ± 2.43*	28.53 ± 2.43	0.31 ± 0.04**

Data are expressed as the means ± duplicates.
Compared with the normal group, $^{\#}P < 0.05$ $^{\#\#}P < 0.01$; compared with the model group, $^{*}P < 0.05$ $^{**}P < 0.01$.

hyperplasia. The smooth muscle cells were slender and the nucleus was rod-shaped.

The uterine smooth muscle layer of the model group had focal hyperplasia, the boundary was unclear, and the local smooth muscle layer was thickened. The cells were obviously enlarged, some mitotic phases appeared, the arrangement was disordered, the nucleus was enlarged, and it was the short fusiform or elliptical shape.

In the positive control levonorgestrel group, the smooth muscle vortex hyperplasia was reduced, most of the smooth muscle layer was slightly thicker, the mouse uterine smooth muscle focal hyperplasia area was significantly reduced, the muscle cells were arranged neatly, and the nuclei were mostly fusiform or rod-shaped. Clinical use of anti-estrogen, progesterone drugs to control the size of myoma to treat uterine fibroids, such as mifepristone tablets and gonadotropin-releasing hormone drugs (Wierman, 2019). In this experiment, levonorgestrel also showed a better inhibitory effect on the proliferation of mouse uterine smooth muscle.

The smooth muscle of the Guizhifuling group showed different degrees of hyperplasia. Most of the muscle cells were hypertrophic and the muscle cells were not arranged neatly. The histopathological histology of the mice in this group was better than that of the model mice.

The OPP high-dose group has a certain inhibitory effect on mouse uterine smooth muscle proliferation. Compared with the model group, smooth intimal hyperplasia was weakened, the muscle cells were arranged more regularly, the muscle layer was thinner, and the nucleus was rod-shaped and similar to the positive drug group. The uterine smooth muscle cells in the medium-dose group were irregularly arranged, and the nucleus was enlarged and oval. In the low-dose group, the uterus of mice had obvious focal hyperplasia of the muscular layer, the arrangement of muscle cells was disordered, and the cells were obviously hypertrophied.

3.5. Endometrial morphology

In Fig. 4C, the endometrium of the normal group was clear and non-proliferative, and glandular epithelial cells were uniform in size. In the model group, the endometrial hyperplasia was obvious, the cells were hypertrophied, and the cystic of the gland was severely dilated. The OPP high-dose group can inhibit the endometrial hyperplasia in mice, and the cell morphology was close to normal; the glandular epithelial cells in the medium-dose group are slightly hypertrophied, the

endometrial hyperplasia in the OPP low-dose group was slightly better than the model. The positive control levonorgestrel group and the Guizhifuling group had obvious inhibitory effects on mouse endometrial hyperplasia. The endometrium of these two groups was clear and the cell morphology was close to normal.

In the data of hyperplasia of smooth muscle, hypertrophy of smooth muscle cells, angiogenesis, endometrial thickening and epithelial hyperplasia in Table 7, each treatment group had a tendency to decrease. Among them, the levonorgestrel group had the most obvious effect, followed by the OPP high dose group.

3.6. Effect on serum E2 in mice

Massart et al. found that the concentration of estrogen and progesterone in uterine fibroids was significantly higher than that in normal uterine smooth muscle tissue (Massart et al., 2014). Compared with the normal control group, the level of serum estradiol (E2) in the model group increased, and the difference was extremely significant ($P < 0.01$), which also indicates that the estrogen-loaded mice were successfully modeled (Fig. 5B). After the model was established and drug intervention, the Western medicine group (Levonorgestrel), the Chinese medicine group (Guizhifuling), the OPP low-dose group, the OPP medium-dose group, and the OPP high-dose group showed a significant decrease in E2 level compared with the model group ($P < 0.01$). The results showed that OPP could reduce E2 level and inhibit the occurrence of uterine fibroids caused by high estrogen. Levonorgestrel had the best effect, while the trend of decreasing E2 level in the OPP high-dose group (57.32 ± 6.78 pg/mL) was obvious, which had no significant difference with the levonorgestrel group (53.45 ± 6.07 pg/mL) ($P > 0.05$).

3.7. Effect on serum P in mice

At present, the specific mechanism of action of hormones in the development of uterine fibroids is not very clear. Hormones can regulate the expression of some growth factors and apoptosis-related factors, which together lead to abnormal proliferation and apoptosis of uterine fibroid cells (Wierman, 2019). For example, in uterine fibroid cells, 17β-estradiol can up-regulate the epidermal growth factor (EGF) receptor and down-regulate p53 protein; while progesterone up-regulates EGF and down-regulates insulin-like growth factor I (IGF-I).
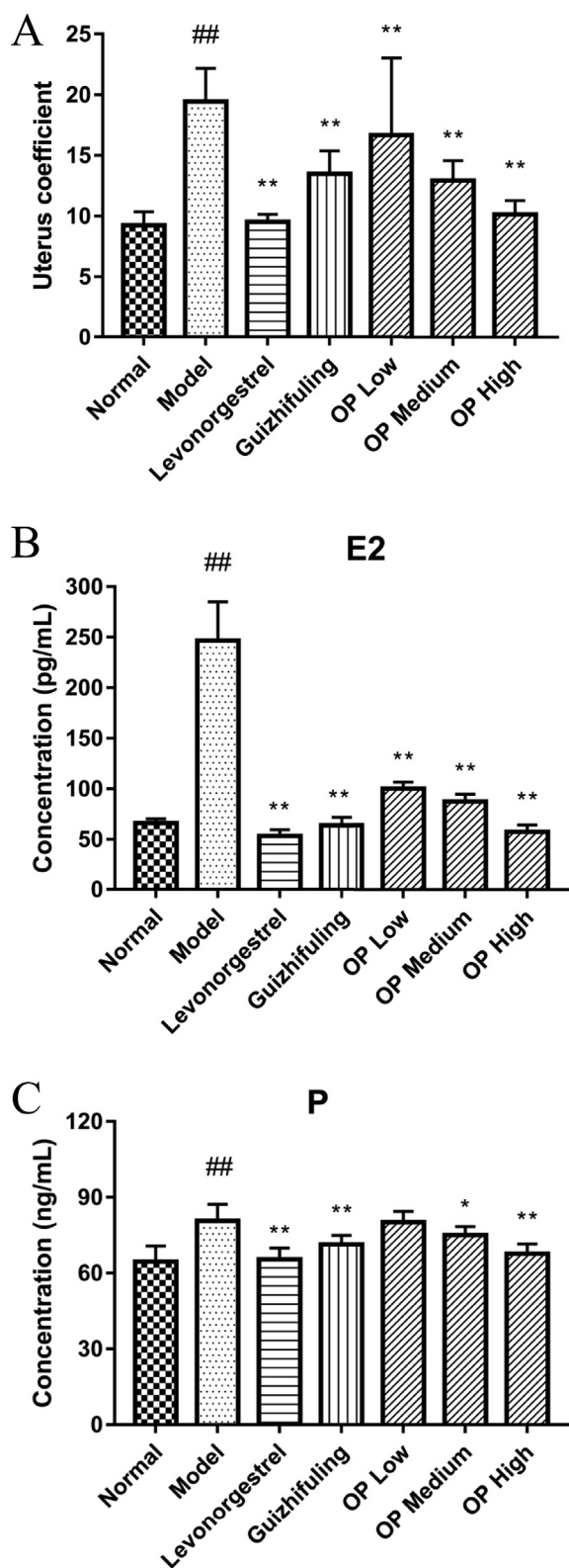
The serum progesterone P concentration in the model group (80.69 ± 6.60 ng/mL) shown in Fig. 5C was very significantly higher than that in the normal group (64.59 ± 6.21 ng/mL) ($P < 0.01$). Compared with the model group, the levels of P in the levonorgestrel group, the Guizhfuling group, and the OPP high-dose group after modeling were significantly decreased ($P < 0.01$). There was a significant difference between the OPP medium-dose group and the model group ($P < 0.05$), indicating that the above groups can reduce the P level. However, the data of the low-dose OPP group (65.48 ± 4.48 ng/mL) was not significantly different from the model group ($P > 0.05$), only the trend of lowering the P level. In summary, it indicated that the OPP as a medicament interfered with the occurrence of uterine fibroids in a dose-dependent manner.

In the study of the effect of the Chinese herbal extract XLS on rat uterine fibroids, Zeng Tao et al. showed that there was no significant difference in serum progesterone (P) concentration between the other groups compared with the normal group (Tao and Yunyi, 2011). They believed that this may be related to the modeling method of estrogen loading alone. The main function of estrogen is to promote the development and maturation of female secondary sexual characteristics, while progesterone hormone is to further promote the development and maturation of secondary sexual characteristics on the basis of estrogen (Gueldini de Moraes et al., 2019). There is a synergistic effect between the two. The mice used in this experiment were modeled and more sensitive to the estrogen of diethylstilbestrol. So the serum progesterone P concentration in the model group was very significantly higher than that in the normal group ($P < 0.01$).

The anti-tumor activity of polysaccharides is mainly achieved by inhibiting the growth of tumor cells, inducing apoptosis, and enhancing immunity. Arabinose had a positive effect on the immune stimulation, galacturonic acid (negative), and arabinose (positive) affected DPPH radical scavenging activity (Yi et al., 2018). All these indicate that the monosaccharide component of OPP has an important effect on the activity. Jin et al. also proved that the higher molecular weight, the stronger anti-complement activity (Jin et al., 2016). At the same time, the high-level structure also affects the activity, as reported by (Yang et al., 2012). Because of the small amount of data, whether these structure–activity relationships are in common needs to be further studied.

4. Conclusion

Through the analysis of 1D (^{1}H NMR and ^{13}C NMR) and 2D (HMBC, COSY, HSQC, and NOESY) NMR spectra, the chemical shifts of each main residue on the methylated derivative obtained by hydrolysis were assigned. Combined with other structural information, it was inferred that the main chain of OPP was connected in the form of 1,3-linked Ara*f*, with a high branching degree and connected with the branch chain at O-2 and O-3 positions, T-Ara*f* and T-Glc*p* were mainly at the end of the main chain. On the other hand, exogenous estrogen was utilized to induce tumor-like hyperplasia of smooth muscle nodules. Under the action of exogenous estrogen for 9 consecutive days, uterus weight and uterus coefficient of the model group were significantly increased compared with the normal group. Pathological sections showed smooth muscle layer thickening, unclear boundaries, enlarged nucleus, short fusiform or elliptical shape, and obvious

Fig. 5 Effect of diethylstilbestrol on mouse uterus coefficient after 9 days of modeling (A). Comparison of serum E2 in mice (B). Comparison of serum P in mice. Compared with the normal group (C), $^{\#}P < 0.05$ $^{\#\#}P < 0.01$; compared with the model group, $^{*}P < 0.05$ $^{**}P < 0.01$.

Table 7 Pathological score of the uterus.

Group	Hyperplasia of smooth muscle	Hypertrophy of smooth muscle cells	Angiogenesis	Endometrial thickening and Epithelial hyperplasia	Sum
Normal	0.10	0.00	0.00	0.00	0.1
Model	2.6	2.6	2.6	2.8	10.6
Levonorgestrel	1.2	1.2	1.2	1.2	4.8
Guizhifuling	1.8	1.9	1.8	1.8	7.3
OPP low dose	2.4	2.2	2.2	2.3	9.1
OPP medium dose	2.0	1.9	1.8	1.9	7.6
OPP high dose	1.5	1.4	1.4	1.4	5.7

According to the hyperplasia of smooth muscle, hypertrophy of smooth muscle cells, angiogenesis, endometrial thickening and epithelial hyperplasia grade: 0-normal, 1-mild, 2-moderate, 3-severe.
Data are expressed as the mean average.

pathological histomorphology changes. The above indicators all suggest that the model is successful. However, due to the short time of modeling, it did not induce the formation of typical uterine fibroids, which were more similar to the early changes before the occurrence of uterine fibroids. The experimental study showed that the high dose group inhibited the uterine fibroids-like hyperplasia induced by diethylstilbestrol in mice, the overall pathological changes were close to normal in the group, the uterine weight and uterine coefficient were significantly reduced, and the serum levels of E2 and P were reduced in a dose-dependent manner.

5. Author agreement

Manuscript is approved by all authors for publication. I would like to declare on behalf of my co-authors that the work described was original research that has not been published previously, and not under consideration for publication elsewhere, in whole or in part.

Declaration of Competing Interest

The authors declare that they have no known competing financial interests or personal relationships that could have appeared to influence the work reported in this paper.

Acknowledgment

No conflict of interest exists in the submission of this manuscript, and the manuscript is approved by all authors for publication.

References

Boggess, J.F., Kilgore, J.E. Tran, A.-Q., 2020. 85 – Uterine Cancer. Abeloff's Clinical Oncology, sixth ed. In: Niederhuber, J.E., Armitage, J.O., Kastan, M.B., et al. (Eds.), Philadelphia, Content Repository Only!, pp. 1508–1524.e1504. https://doi.org/10.1016/B978-0-323-47674-4.00085-2.

Chen, L., Huang, G., 2017. Antitumor activity of polysaccharides: an overview. Curr. Drug Targets 18. https://doi.org/10.2174/1389450118666170704143018.

Chen, L., Zhao, X., Wu, J.E., et al, 2020. Metabolic characterisation of eight Escherichia coli strains including "Big Six" and acidic responses of selected strains revealed by NMR spectroscopy. Food Microbiol. 88. https://doi.org/10.1016/j.fm.2019.103399.

Cui, H.X., 2012. Antitumor activity and possible mechanism of crude polysaccharides from Discorea bulbifera L. on the mice bearing U14 cervical carcinoma. Adv. Mater. Res. 560–561, 374–379. https://doi.org/10.4028/www.scientific.net/AMR.560-561.374.

Dai, J.F., Lei, L.I., 2001. Analysis for the composition of monosaccharide in the polysaccharide from Osmunda japonica Thunb. Acta Agriculturae Universitis Jiangxiensis 04, 492–494. https://doi.org/10.13836/j.jjau.2001120.

Dai Jinfeng, L.L., Hui, L., Hainan, T., 1999. Research progress of Osmunda japonica Thunb. Chin. Tradit. Herbal Drugs 717–719. https://doi.org/10.7501/j.issn.0253-2670.1999.9.511.

Dongyun, L., 2010. Clinical observation on 60 cases of uterine myoma treated with guizhifuling capsule 2845-2845 Jilin Med. College 31. https://doi.org/10.3969/j.issn.1004-0412.2010.18.060.

Fan, Z., Che, H., Yang, S., et al, 2019. Estrogen and estrogen receptor signaling promotes allergic immune responses: effects on immune cells, cytokines, and inflammatory factors involved in allergy. Allergol. Immunopathol. 47, 506–512. https://doi.org/10.1016/j.aller.2019.03.001.

Fimbres-Olivarria, D., Carvajal-Millan, E., Lopez-Elias, J.A., et al, 2018. Chemical characterization and antioxidant activity of sulfated polysaccharides from Navicula sp. Food Hydrocolloids 75, 229–236. https://doi.org/10.1016/j.foodhyd.2017.08.002.

Gueldini de Moraes, A.V., Ribeiro Valadares, A.L., Lui Filho, J.F., et al, 2019. Medication use and sexual function: a population-based study in middle aged women. J. Sex. Med. 16, 1371–1380. https://doi.org/10.1016/j.jsxm.2019.06.004.

He, B.-L., Zheng, Q.-W., Guo, L.-Q., et al, 2020. Structural characterization and immune-enhancing activity of a novel high-molecular-weight polysaccharide from Cordyceps militaris. Int. J. Biol. Macromol. 145, 11–20. https://doi.org/10.1016/j.ijbiomac.2019.12.115.

Ji, X., Hou, C., Yan, Y., et al, 2020. Comparison of structural characterization and antioxidant activity of polysaccharides from jujube (Ziziphus jujuba Mill.) fruit. Int. J. Biol. Macromol. 149, 1008–1018. https://doi.org/10.1016/j.ijbiomac.2020.02.018.

Ji, X., Liu, F., Peng, Q., et al, 2018. Purification, structural characterization, and hypolipidemic effects of a neutral polysaccharide from Ziziphus Jujuba cv. Muzao. Food Chem. 245, 1124–1130. https://doi.org/10.1016/j.foodchem.2017.11.058.

Jin, W.H., Zhang, W.J., Liang, H.Z., et al, 2016. The structure-activity relationship between marine algae polysaccharides and anti-complement activity. Mar. Drugs 14, 3. https://doi.org/10.3390/md14010003.

Li Lei, T.H., 1999. Isolation, purification and basic properties of Osmunda japonica Thunb polysaccharide POJI. Food Sci. 20, 11–14. https://doi.org/10.1017/S0266078400010713.

Li, Y., Shi, L., 2014. Effect of desiccation level and storage temperature on green spore viability of Osmunda japonica.

Cryobiology 68, 446–450. https://doi.org/10.1016/j.cryobiol.2014.03.002.

Liao, T.-L., Lee, Y.-C., Tzeng, C.-R., et al, 2019. Mitochondrial translocation of estrogen receptor β affords resistance to oxidative insult-induced apoptosis and contributes to the pathogenesis of endometriosis. Free Radical Biol. Med. 134, 359–373. https://doi.org/10.1016/j.freeradbiomed.2019.01.022.

Liu, X., Zhang, X., Zhang, X., et al, 2020a. Antibacterial activity of Osmunda japonica (Thunb) polysaccharides and its effect on tomato quality maintenance during storage. Int. J. Food Sci. Technol. 55, 2851–2862. https://doi.org/10.1111/ijfs.14541.

Liu, X., Zhang, X., Zhang, X., et al, 2020b. Effects of different drying methods on the physicochemical and antioxidative characteristics of Osmunda japonica Thunb. polysaccharides. J. Food Process. Preserv. 44, e14742. https://doi.org/10.1111/jfpp.14742.

Liu, X.C., Yu, X.H., Zhang, X.T., et al, 2021. Preparation of polysaccharides from Osmunda japonica (Thunb) with the potential of food additives: structural features and functional properties. J. Food Process. Preserv. 45, e15189. https://doi.org/10.1111/jfpp.15189.

Liu, Y., Wang, S., Kang, J., et al, 2020c. Arabinoxylan from wheat bran: molecular degradation and functional investigation. Food Hydrocolloids 107, 105914. https://doi.org/10.1016/j.foodhyd.2020.105914.

Lv, Q.-Q., Cao, J.-J., Liu, R., et al, 2021. Structural characterization, α-amylase and α-glucosidase inhibitory activities of polysaccharides from wheat bran. Food Chem. 341, 128218. https://doi.org/10.1016/j.foodchem.2020.128218.

Ma Jun, X.R., Xiaodong, W., et al, 2008. Study on the effect of Qinggongliu Pill on uterine leiomyoma. J. Gansu College Tradit. Chin. Med. 25, 8–10. https://doi.org/10.3969/j.issn.1003-8450.2008.03.003.

Massart, S., Milla, S., Kestemont, P., 2014. Expression of gene, protein and immunohistochemical localization of the estrogen receptor isoform ERα1 in male rainbow trout lymphoid organs; indication of the role of estrogens in the regulation of immune mechanisms. Comp. Biochem. Physiol. B: Biochem. Mol. Biol. 174, 53–61. https://doi.org/10.1016/j.cbpb.2014.06.001.

Mohamed, S., Ayman, A.H., 2012. Medical treatment of uterine leiomyoma. Reprod. Sci. 19, 339–353. https://doi.org/10.1177/1933719111432867.

Nini, C., Mei, H., Hong, Y., et al, 2014. Chinese herbal medicine guizhi fuling formula for treatment of uterine fibroids: a systematic review of randomized clinical trials. J. Altern. Comp. Med. 14, 2. https://doi.org/10.1186/1472-6882-14-2.

Qi, S., Weijing, Y., Xiaoli, H., et al, 2016. The effects of Guizhi Fuling capsule drug serum on uterine leiomyoma cells and its mechanism. Evid. Comp. Alternat. Med. 2016, 1–9. https://doi.org/10.1155/2016/2393640.

Tao, Y.-W., Tian, G.-Y., 2006. Studies on the physicochemical properties, structure and antitumor activity of polysaccharide YhPS-1 from the root of Cordalis yanhusuo Wang. Chin. J. Chem . 24, 235–239. https://doi.org/10.1002/cjoc.200690045.

Tao, Z., 2011. Anti-inflammatory and blood-activating effects of anti-uterine fibroids Chinese herbal extract XLS. Chin. J. Clin. Pharm. 20, 141–143. https://doi.org/10.19577/j.cnki.issn10074406.2011.03.004.

Tian, R., Cheng, C., Wang, X.P., 2011. Analysis and evaluation of nutrients in wild and cultivated species of Osmunda japonica Thunb. Food Sci. 32, 297–300. https://doi.org/10.3724/SP.J.1011.2011.00187.

Wan, Z., Fang, J., 2000. Application of nuclear magnetic resonance spectroscopy in the structural determination of polysaccharide. Chin. J. Anal. Chem. 28, 240–247. https://doi.org/10.1016/S0003-2670(99)00851-X.

Wang, H.-B., 2014. Cellulase-assisted extraction and antibacterial activity of polysaccharides from the dandelion Taraxacum officinale. Carbohydr. Polym. 103, 140–142. https://doi.org/10.1016/j.carbpol.2013.12.029.

Wierman, M.E., 2019. Gonadotropin-Releasing Hormone (GnRH) Development and Actions. Encyclopedia of Endocrine Diseases, second ed. In: Huhtaniemi, I., Martini, L. (Eds.). Oxford, Academic Press, pp. 692–694. https://doi.org/10.1016/B978-0-12-801238-3.95842-2.

Yang, D., Lin, F., Huang, Y., et al, 2020. Separation, purification, structural analysis and immune-enhancing activity of sulfated polysaccharide isolated from sea cucumber viscera. Int. J. Biol. Macromol. 155, 1003–1018. https://doi.org/10.1016/j.ijbiomac.2019.11.064.

Yang, W., Pei, F., Shi, Y., et al, 2012. Purification, characterization and anti-proliferation activity of polysaccharides from Flammulina velutipes. Carbohydr. Polym. 88, 474–480. https://doi.org/10.1016/j.carbpol.2011.12.018.

Yi, Y., Lamikanra, O., Sun, J., et al, 2018. Activity diversity structure-activity relationship of polysaccharides from lotus root varieties. Carbohydr. Polym. 190, 67–76. https://doi.org/10.1016/j.carbpol.2017.11.090.

You, Q., Yin, X., Zhang, S., et al, 2014. Extraction, purification, and antioxidant activities of polysaccharides from Tricholoma mongolicum Imai. Carbohydr. Polym. 99, 1–10. https://doi.org/10.1016/j.carbpol.2013.07.088.

Yuan, Q., Lin, S., Fu, Y., et al, 2019. Effects of extraction methods on the physicochemical characteristics and biological activities of polysaccharides from okra (Abelmoschus esculentus). Int. J. Biol. Macromol. 127, 178–186. https://doi.org/10.1016/j.ijbiomac.2019.01.042.

Zhao, C., Li, X., Miao, J., et al, 2017. The effect of different extraction techniques on property and bioactivity of polysaccharides from Dioscorea hemsleyi. Int. J. Biol. Macromole. 102, 847–856 https://doi.org/10.1016/j.ijbiomac.2017.04.031.

Zhao, H.-K., Wei, X.-Y., Xie, Y.-M., et al, 2019. Preparation of nanocellulose and lignin-carbohydrate complex composite biological carriers and culture of heart coronary artery endothelial cells. Int. J. Biol. Macromol. 137, 1161–1168. https://doi.org/10.1016/j.ijbiomac.2019.07.062.